ISBN: 978-3-95450-211-0 doi:10.18429/JACoW-SRF2019-THP020

STUDY OF DISLOCATION CONTENT NEAR GRAIN BOUNDARIES USING ELECTRON CHANNELING CONTRAST IMAGING AND ITS EFFECT ON THE SUPERCONDUCTING PROPERTIES OF NIOBIUM*

M. Wang, T. Bieler†, Chemical Engineering and Materials Science
Michigan State University, East Lansing, MI 48824, USA
S. Balachandran, S. Chetri, A. A. Polyanskii, P. J. Lee, Applied Superconductivity Center
National High Magnetic Field Laboratory, Florida State University, Tallahassee, FL 32310, USA
C.C. Compton, Facility for Rare Isotope Beams, East Lansing, MI 48824, USA

Abstract

Trapped micro-Tesla levels of magnetic flux degrade the performance of Nb superconducting radio frequency (SRF) accelerators. Recent studies have revisited the role of small deformation (dislocation substructure influence) on cavity performance. However, the link between microstructural defects and mechanisms leading to poor performance is still unresolved. To examine the mechanism of flux pinning by dislocations and grain boundaries, bi-crystal Nb tensile samples were designed with strategically chosen tensile axes to favor introduction of dislocation content near grain boundaries by a small tensile strain. Dislocation structures near the grain boundaries were characterized before and after 5% tensile deformation using electron channeling contrast imaging (ECCI), after which the magnetic flux behavior was observed using cryogenic magneto-optical (MO) imaging. The conditions which increase the tendency to trap flux in regions of high dislocation density of one Nb bi-crystal are discussed.

INTRODUCTION

High purity niobium (RRR>300) has been used for fabrication of particle accelerator cavities due to its superconductivity [1] . Great advancements on pursuing higher quality factor (Q) and accelerating gradient have been achieved in the past decades [2–4] in the superconductivity radio frequency (SRF) community. However, the SRF cavity performance is still limited by the variability of the niobium material, resulting from various factors including the anisotropic mechanical properties and dislocation substructures. The long path of fabrication and processing of niobium cavities introduces microstructural defects (dislocations and grain boundaries, GB) into the material, which could act as pinning centers causing flux pinning at superconducting temperatures and, as a result, degrade the cavity performance and energy efficiency [3, 5–11]. Even in undeformed high purity Nb samples, there are a large number of pre-existing dislocations ($\rho \sim 9\times10^{12}m^{-2}$), which can affect flow stress behavior during subsequent deformation [12–14].

To study the effect of dislocations and grain boundaries on magnetic flux trapping, tensile samples were designed with strategically chosen tensile axes to favor introduction of dislocations near grain boundaries after 5% tensile deformation. Electron channeling contrast imaging (ECCI) was used to examine the dislocation structures near grain boundaries. ECCI has the advantage of minimal surface preparation, compared with TEM, and provides large areas for investigation. The magnetic flux behavior was observed using Magneto-optical (MO) imaging. In this paper, the results of one bi-crystal sample are presented and discussed.

SAMPLE DESIGN

Dislocation Slip

Dislocation slip enables the formability of metals through the activation of slip systems under applied shear stress. There are 48 slip systems for Nb, each of them having a specified slip plane and slip direction. When a shear stress is applied, the resolved shear stress on these slip systems will be different, and the ones with the highest resolved shear stress will be most likely to be activated. This likelihood can be described by Schmid factor, a value ranging from 0 to 0.5, with 0.5 representing the highest likelihood of activation during deformation. The calculation of the Schmid factor was used to guide the choice of the tensile axis.

Tensile Axis Choosing

Tensile samples were extracted from a 3 mm thick high-purity (RRR>300) large-grain Nb disk. The tensile axis was chosen to cause focused shear deformation along the GB so that their effect on flux trapping can be evaluated. In order to achieve this goal, a MATLAB code was developed to calculate Schmid factors of all slip systems in Nb based on crystal orientations measured using Laue X-ray diffraction. The tensile axis was rotated by 360°, and the Schmid factor calculation was made for each degree of rotation in order to find a slip system parallel to the GB with a high likelihood of activation when deformed along chosen axis.

The surface normal direction orientation map of the Nb disk is shown in Figure 1a, which is color coded based on the crystal directions that are parallel to the surface normal. Figure 1b shows the layout of two tensile samples overlaid

* Supported by the U.S. Department of Energy (Award Numbers DE-FG02-13ER41974, DE-SC0009962 and DE-SC0009960). A portion of this work was performed at the National High Magnetic Field Laboratory, supported by National Science Foundation Cooperative Agreement No. DMR-1157490 (-2017) DMR-1644779 (2018-) and the State of Florida. Material and some specimen preparations were provided by FRIB.
† bieler@egr.msu.edu

ISBN: 978-3-95450-211-0 doi:10.18429/JACoW-SRF2019-THP020

on a portion of the Nb disk. The overlaid unit cell prisms represent the orientations and chosen slip systems of grains 6, 9, and 10, with shaded planes representing the slip planes, and torquoise lines the slip directions or Burgers vectors. Schmid factors are listed for the four most favored slip systems in each grain in the lower table in Figure 1b. It shows that for the chosen tensile axes of samples GB6-10 and GB10-9, each grain has highly favored slip systems, and both grain 6 and grain 9 have a slip system parallel to the GB. In this paper, the results of sample GB10-9 are presented.

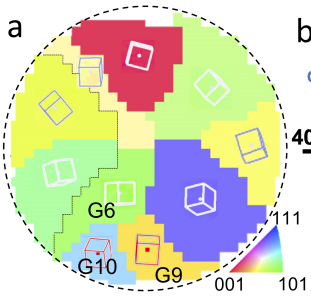

	Schmid factor			
Grain 6	0.5	0.44	0.42	0.35
Grain 9	0.5	0.47	0.46	0.45
Grain 10	0.48	0.48	0.45	0.45

Figure 1: a) Normal direction orientation map of a large-grain Nb disk, color coded based on the crystal directions parallel to the surface normal; b) Portion of the Nb disk overlaid with drawings of tensile samples GB6-10 and GB10-9 with chosen tensile axes and prisms representing crystal orientations and most favored slip systems. The lower table shows the Schmid factors for the four most favored slip systems in grain 6, 9, and 10, for the chosen tensile axes.

CHARACTERIZATION METHODS

Electron Channeling Contrast Imaging (ECCI)

ECCI is a SEM (Scanning Electron Microscope) based technique that enables dislocation imaging [15–18]. A dislocation changes the local lattice orientation in an otherwise perfect crystal lattice, resulting in a contrast change in the backscattered electron (BSE) signal used to form ECCI dislocation images. ECCI has advantages of a large observation area, bulk sample observation, and non-destructive sample preparation. Most importantly, surface preparation for ECCI only requires a good polish, so SRF cavity coupons can be characterized for deformation microscopic structures. In contrast, TEM sample preparation could lead to modifications of the microstructure.

To obtain an ECCI dislocation image, the sample was rotated and tilted into channeling conditions when the electron beam axis is at the edge of a channeling band, as shown in Figure 2a and c, where the red dot represents the electron beam axis. The parallel white dashed lines mark the chosen channeling bands, with diffraction vectors g denoted. Under channeling conditions, dislocation images can be collected using a BSE dector in SEM, as shown in Figure 2b and 2d. These are dislocation images of the same area under two different channeling conditions **g** = (-1-1-2) and **g** = (200). Dislocation visibility changes with channeling conditions, which can be used for contrast analysis to identify dislocation characters [17].

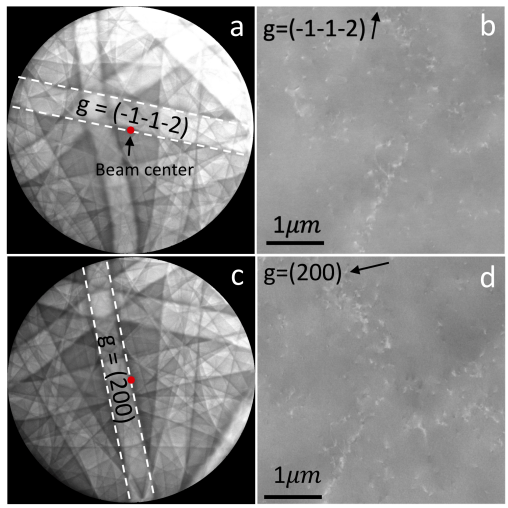

Figure 2: Channeling patterns (a and c) and the corresponding dislocation images (b and d) of the same location on Nb sample surface under different channeling conditions. Note the beam center (red dot) is at the edge of the g = (-1-1-2) band for the first channeling condition (upper), and at the edge of the g = (200) band for the second channeling condition (lower). Different dislocations are visible or invisible in these two conditions.

Magneto-Optical (MO) Imaging

MO imaging can reveal locations of magnetic flux trapping or penetration, which could cause local superconductivity suppression due to defects in Nb [19, 20]. This method is based on the Faraday effect, where polarized light is rotated by a magnetic field. In MO images, a bright contrast corresponds to higher magnetic flux density. The setup of MO imaging is shown in Figure 3.

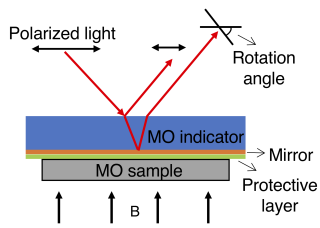

Figure 3: Setup of MO imaging for magnetic flux observation.

RESULTS

Flux Trapping in One Grain

After 5% tensile deformation, an MO sample with a diameter of 3mm and a thickness of 1.5mm was extracted from the bi-crystal GB of the deformed tensile sample GB10-9, as shown in Figure 4a, where the red dashed line denotes the location of the GB. The optical image and MO image

ISBN: 978-3-95450-211-0 doi:10.18429/JACoW-SRF2019-THP020

of the extracted MO sample are shown in Figure 4b and c, respectively.

The MO image was taken following a field cooled condition, where the sample was cooled in an external magnetic field of 120 mT. This field was reduced to zero after the temperature reached 6.4K (below the critical temperature T_c), and then the MO image was taken at H = 0 mT. In the MO image (Figure 4c), the left grain shows a brighter contrast than the right grain, indicating more flux trapping in the left grain.

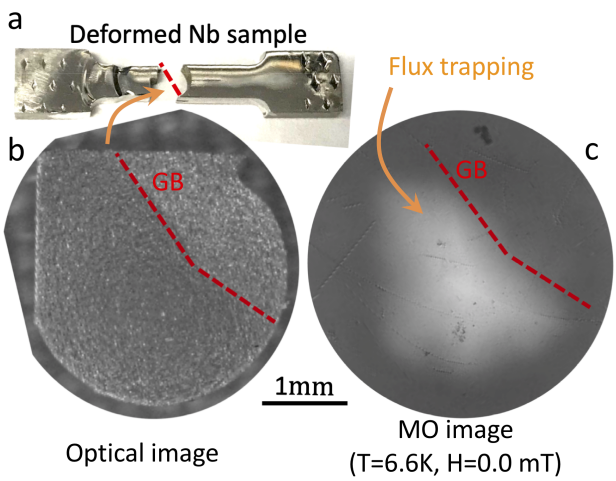

Figure 4: MO sample extracted from the deformed tensile sample (a) and its optical image (b) and field cooled MO image (c). The left grain shows more flux trapping than the right grain.

Dislocation Density

In order to identify the microstructure effect on flux trapping observed in MO imaging (Figure 4), ECCI was performed in both grains of the bi-crystal sample GB10-9 and the dislocation images of two different regions in each grain are shown in Figure 5, where the white or dark features are dislocations with dislocation lines at different angles from the sample surface. By counting these features (excluding dislocations in low angle grain boundaries) and dividing this number by the area, the density of dislocations can be estimated. It is worth noting that this counting is the lower bound of dislocation density, because (1) not all dislocations are visible under chosen channeling conditions, and (2) not all observed dislocations are perpendicular to the surface. Thus, a geometry correction proposed in ref [21] was used to make a better estimate of the measured dislocation density, assuming the dislocations are is random orientations. A correction factor of 1/cos(60°) was multiplied by the measured dislocation density values.

The dislocation densities measured from five areas in each of the left and the right grain are shown in the bar plot in Figure 6. The left grain has a higher density of dislocations, corresponding to the higher flux trapping revealed by MO imaging (Figure 4), suggesting the existence of a correlation between flux trapping and dislocation content.

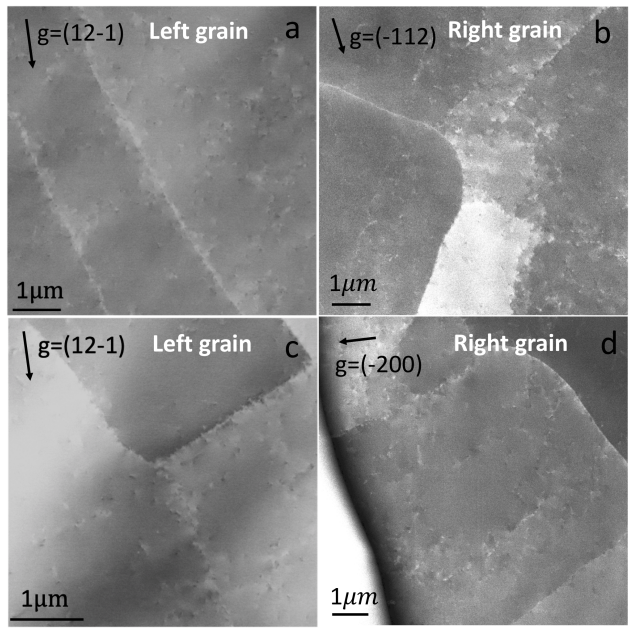

Figure 5: Dislocation images of two regions of the left grain (a and c) and the right grain (b and d) of bi-crystal GB10-9. Both high density dislocations (white and dark features) and low angle grain boundaries can be observed.

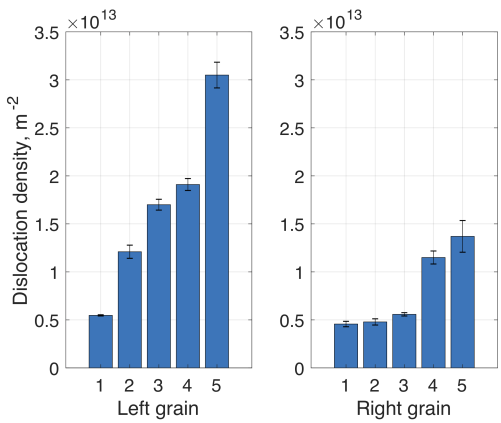

Figure 6: Dislocation density estimation from ECCI images: the left grain has a higher density of dislocations.

Sub-Grain Development After Deformation

Low angle grain boundaries (LAGBs) were observed in dislocation images of both grains (Figure 5) after 5% deformation. During the deformation, dislocations are generated and then organized to form low-energy dislocation walls, or LAGBs, to accommodate the deformation [22]. These LAGBs, which are composed of dislocations, can be imaged using ECCI. Figure 7 shows the comparison of ECCI images of the same area in the right grain before and after 5% deformation. Compared with the before deformation image Figure 7a, the after deformation image Figure 7b shows more developed LAGBs, indicating sub-grain development during the 5% deformation.

ISBN: 978-3-95450-211-0 doi:10.18429/JACoW-SRF2019-THP020

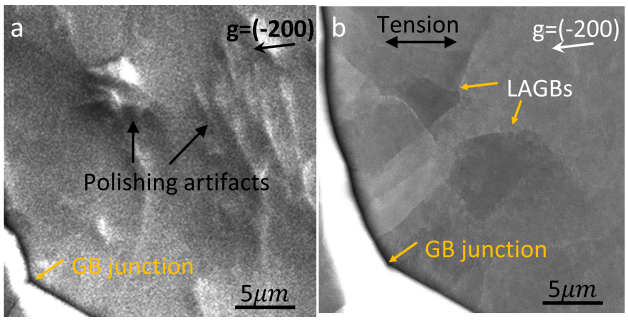

Figure 7: ECCI images of the same area in the right grain near the grain boundary junction before (a) and after (b) deformation show trend of sub-grain development.

Dislocation slip during plastic deformation leads to crystal rotation, and hence, local crystal orientation changes leading to local misorientations, which can be measured using electron backscatter diffraction (EBSD) before and after deformation. Based on EBSD data, the grain reference orientation deviation (GROD) maps can be generated to show the trend of orientation evolution during deformation. Using the average grain orientation as a reference, the data can be plotted either as orientation deviation angle maps (Figure 8a and b), or as rotation axis maps (Figure 8c and d), where maps (a) and (c) show the before deformation condition, and (b) and (d) show the change after deformation. The GROD angle maps (a) and (b) show a lower orientation deviation after deformation, indicating that dislocations could exit the sample or accumulate in LAGBs after deformation. Maps (c) and (d) show that local regions rotate about a particular rotation axis after deformation (Figure 8d), consistent with sub-grain development observed from ECCI images in Figure 7.

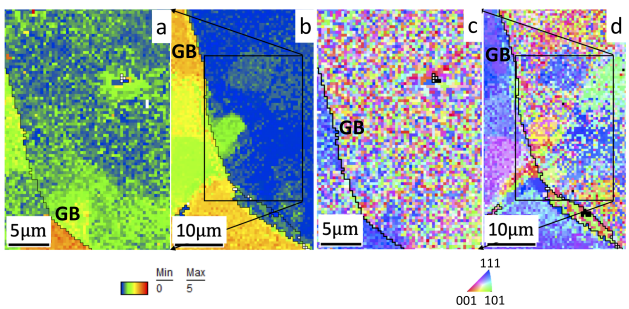

Figure 8: Grain reference orientation deviation map of the right grain before (a) and after deformation (b) shows more distinct regions with specific grain orientations and sharper boundaries with different orientations after deformation. (c) shows no prior local preferred rotation axes before deformation, but in (d), there are regions with distinct misorientation axis after deformation, indicating that different sub-grain boundaries consist of dislocations operating on different slip planes.

DISCUSSION

This study demonstrates the capability of ECCI to image individual dislocations and quantify dislocation densities in deformed Nb, and how MO imaging technique can be used to assess the correlation between flux trapping and dislocation content. The large observation area in bulk samples facilitates meaningful statistical studies of dislocation structures using ECCI in deformed Nb samples. ECCI can also be used with in situ characterization to identify evolution of dislocation characters and the development of LAGBs in deformed samples.

A sampling of dislocation densities using ECCI in both grains in bi-crystal GB10-9 clearly shows that the left grain has a higher density of dislocations after 5% tensile deformation. A higher dislocation density corresponds with higher flux trapping, as revealed by the MO imaging. This result suggests that free dislocations cause local suppression of superconductivity and degrade the Nb cavity performance. However, it is not known how LAGB dislocation structures correlate with flux trapping as distinguished from free dislocations between LAGBs. Furthermore, MO imaging is not able to resolve individual dislocation flux trapping, making it difficult to distinguish between flux trapping by individual dislocations and LAGBs.

LAGBs have a low misorientation angle (<15°) and consist of dislocations that can be imaged. ECCI observation in the right grain (Figure 7b) shows the development of distinct sub-grains or LAGBs after deformation. This is consistent with the grain reference orientation deviation maps (Figure 8), which show that local regions have different rotation axes, resulting from dislocation slip on different slip systems that interact to form LAGBs, or sub-grains. Prior work shows that LAGBs are also capable of trapping magnetic flux and disturb superconducting currents [23].

CONCLUSION

This paper demonstrates the capability of ECCI to characterize individual dislocations and quantify dislocation densities in deformed Nb samples, which were designed with chosen tensile axes to favor introduction of dislocation content near grain boundaries during deformation. ECCI combined with MO imaging enables the study of the correlation between dislocation content and magnetic flux trapping in lightly deformed Nb samples in order to achieve further understanding of the mechanism of flux trapping by microstructural defects such as dislocations and grain boundaries.

The combination of MO imaging and ECCI analysis shows correlation between dislocation density and magnetic flux trapping. This implies that dislocations can trap magnetic flux and degrade superconductivity of Nb.

Both ECCI and EBSD analysis show well-developed orientation gradients and LAGBs following deformation. Dislocations and low angle grain boundaries can cause flux trapping and degrade the performance of SRF cavities. Therefore materials processing methods need to be developed to remove as many dislocations and LAGBs as possible.

ISBN: 978-3-95450-211-0 doi:10.18429/JACoW-SRF2019-THP020

REFERENCES

[1] W. Singer, "SRF Cavity Fabrication and Materials," in *arXiv*, vol. 1501.07142, May 2013. Erice, Italy: CERN, 2015, pp. 171–207. http://arxiv.org/abs/1501.07142, doi:10.5170/CERN-2014-005.171

[2] K. Saito,"State-of-the-Art and Future Prospects in RF Superconductivity", in *Proc. IPAC'12*, New Orleans, LA, USA, May 2012, paper MOYBP01, pp. 11–15.

[3] T. R. Bieler, N. T. Wright, F. Pourboghrat, C. Compton, K. T. Hartwig, D. Baars, A. Zamiri, S. Chandrasekaran, P. Darbandi, H. Jiang, E. Skoug, S. Balachandran, G. E. Ice, and W. Liu, "Physical and mechanical metallurgy of high purity Nb for accelerator cavities," *Physical Review Special Topics - Accelerators and Beams*, vol. 13, no. 3, p. 31002, 2010. doi:10.1103/PhysRevSTAB.13.031002

[4] G. Ciovati, "Effect of low-temperature baking on the radio-frequency properties of niobium superconducting cavities for particle accelerators," *Journal of Applied Physics*, vol. 96, no. 3, pp. 1591–1600, 2004.

[5] G. Ciovati and A. Gurevich, "Measurement of RF Losses Due to Trapped Flux in a Large-Grain Niobium Cavity", in *Proc. SRF'07*, Beijing, China, Oct. 2007, paper TUP13, pp. 132–136.

[6] T. Matsushita, *Flux Pinning in Superconductors*, New York: Springer, 2007, vol. 164.

[7] G. Ciovati and A. Gurevich, "Evidence of high-field radio-frequency hot spots due to trapped vortices in niobium cavities," *Physical Review Special Topics - Accelerators and Beams*, vol. 11, no. 12, p. 122001, 2008. doi:10.1103/PhysRevSTAB.11.122001

[8] A. Dasgupta, C. C. Koch, D. M. Kroeger, and Y. T. Chou, "Flux pinning by grain boundaries in niobium bicrystals," *Philosophical Magazine Part B*, vol. 38, no. 4, pp. 367–380, 1978. doi:10.1080/13642817808245338

[9] G. Zerweck, "On pinning of superconducting flux lines by grain boundaries," *Journal of Low Temperature Physics*, vol. 42, no. 1-2, pp. 1–9, 1981. doi:10.1007/BF00116692

[10] M. Checchin, M. Martinello, A. Romanenko, A. Grassellino, D. A. Sergatskov, S. Posen, O. Melnychuk, and J. F. Zasadzinski, "Quench-Induced Degradation of the Quality Factor in Superconducting Resonators," *Physical Review Applied*, vol. 5, no. 4, p. 44019, 2016. doi:10.1103/PhysRevApplied.5.044019

[11] S. Posen, M. Checchin, A. C. Crawford, A. Grassellino, M. Martinello, O. S. Melnychuk, A. Romanenko, D. A. Sergatskov, and Y. Trenikhina, "Efficient expulsion of magnetic flux in superconducting radiofrequency cavities for high Q0 applications," *Journal of Applied Physics*, vol. 119, no. 21, p. 213903, 2016. doi:10.1063/1.4953087

[12] M. Wang, D. Kang, and T. R. Bieler, "Direct observation of dislocation structure evolution in SRF cavity niobium using electron channeling contrast imaging," *Journal of Applied Physics*, vol. 124, no. 15, p. 155105, 2018.

[13] M. Wang, T. Bieler, C. Compton, and D. Kang, "Characterization of Microstructural Defects in SRF Cavity Niobium using Electron Channeling Contrast Imaging", in *Proc. SRF'17*, Lanzhou, China, Jul. 2017, pp. 792–796. doi:10.18429/JACoW-SRF2017-THPB027

[14] D. Kang, D. Baars, T. Bieler, C. Compton, A. Mapar, and F. Pourboghrat, "Study of Slip and Deformation in High Purity Single Crystal Nb for Accelerator Cavities", in *Proc. SRF'15*, Whistler, Canada, Sep. 2015, paper MOPB045, pp. 191–195.

[15] M. A. Crimp, "Scanning electron microscopy imaging of dislocations in bulk materials, using electron channeling contrast," *Microscopy Research and Technique*, vol. 69, no. 5, pp. 374–381, 2006.

[16] B. A. Simkin and M. A. Crimp, "An experimentally convenient configuration for electron channeling contrast imaging," *Ultramicroscopy*, vol. 77, no. 1–2, pp. 65–75, 1999.

[17] M. A. Crimp, B. A. Simkin, and B. C. Ng, "Demonstration of the g·bxu= 0 edge dislocation invisibility criterion for electron channelling contrast imaging," *Philosophical magazine letters*, vol. 81, no. 12, pp. 833–837, 2001.

[18] S. Zaefferer and N.-N. Elhami, "Theory and application of electron channelling contrast imaging under controlled diffraction conditions," *Acta Materialia*, vol. 75, pp. 20–50, 2014.

[19] A. A. Polyanskii, P. J. Lee, A. Gurevich, Z.-H. Sung, D. C. Larbalestier, G. R. Myneni, G. Ciovati, and M. Stuart, "Magneto-Optical Study High-Purity Niobium for Superconducting RF Application," in *AIP Conference Proceedings-American Institute of Physics*, vol. 1352, no. 1, 2011, pp. 186–202.

[20] A. A. Polyanskii, A. Gurevich, A. E. Pashitski, N. F. Heinig, R. D. Redwing, J. E. Nordman, and D. C. Larbalestier, "Magneto-optical study of flux penetration and critical current densities in [001] tilt YBa2Cu3O7 δ thin-film bicrystals," *Physical Review B*, vol. 53, no. 13, p. 8687, 1996.

[21] M. Crimp, J. Hile, T. Bieler, and M. Glavicic, "Dislocation density measurements in commercially pure titanium using electron channeling contrast imaging," *TMS Lett*, vol. 1, pp. 15–16, 2004.

[22] T. R. Bieler, S. C. Sutton, B. E. Dunlap, Z. A. Keith, P. Eisenlohr, M. A. Crimp, and B. L. Boyce, "Grain boundary responses to heterogeneous deformation in tantalum polycrystals," *JOM*, vol. 66, no. 1, pp. 121–128, 2014.

[23] M. Wang, S. Balachandran, T. Bieler, S. Chetri, C. Compton, P. Lee, and A. Polyanskii,"Investigation of the Effect of Strategically Selected Grain Boundaries on Superconducting Properties of SRF Cavity Niobium", in *Proc. SRF'17*, Lanzhou, China, Jul. 2017, pp. 787–791. doi:10.18429/JACoW-SRF2017-THPB026